ELSEVIER

Ultrasonics 39 (2001) 109–113

Ultrasonics

www.elsevier.nl/locate/ultras

The role of internal reflection in transskull phase distortion

G.T. Clement *, Jie Sun, Kullervo Hynynen

Department of Radiology, Brigham and Women's Hospital, Harvard Medical School, 75 Francis St., Boston, MA 02115, USA

Received 1 June 2000; received in revised form 22 June 2000

Abstract

Phase distortion due to reflection in transcranial ultrasound propagation is investigated. Understanding of these phase-dependent properties is motivated by efforts to construct a reliable prediction model for noninvasive ultrasound therapy in the brain. The present study measures the phase of an ultrasound wave after propagation through an ex vivo human skull and considers the dependence of this phase on reflections between the transducer and the skull surface in addition to reflections within the skull. Experiments are performed using a human calvarium fragment placed between an underwater ultrasonic transducer and a polyvinylidene difluoride hydrophone. Data are presented indicating the ultrasound phase dependence as a function of burst length and the distance of the transducer element from the skull at a driving frequency of 0.5 MHz. Experimental results are compared with predictions obtained from a propagation model which considers transmission at the skull interfaces as well as multiple reflections within the skull. It is concluded that by using short ultrasound bursts a distance may be indicated that beyond which the contributions of transducer reflections on the phase of the propagating wave may be neglected. Additionally, a comparison of the measurements with simulated data supports the contention that for reasonably small incident angles, reflection within the skull causes minimal phase shift.

Keywords: Ultrasound surgery; Phased arrays; Cancer therapy

1. Introduction

Advances in transducer array and amplifier technology have prompted proposals for both mildly-invasive and noninvasive techniques for ultrasound surgery through the skull [1,2]. A procedure of this type is contingent upon a reliable model for predicting the physical response of the skull to sonication. The model must function using information available from a noninvasive diagnostic procedure. For example, a prediction of the location and size of the focal region could be made from knowledge of the position, thickness, and orientation of the inner and outer surfaces of the skull; all quantities that could be obtained in vivo using MRI, or other noninvasive diagnostic methods.

The predominant control factor for reconstructing the ultrasound focus with a multi-element array is the acoustic phase [3,4]. That is, a focused beam distorted by diffraction and attenuation while propagating through the skull bone may be refocused by adjusting the driving phase of each element. While for a single source transducer the driving phase has no control over the acoustic intensity, by wave superposition it is the primary source for determining a focus with an array of sources; e.g. two high amplitude sources focused on the same point but π radians out of phase produce a null focal point. It follows that driving phases be chosen such that the pressure field of each element arrives at the intended focal point in phase. Noninvasive focusing through the skull thus requires a phase prediction model that includes any factors causing an appreciable change in the ultrasound phase. The present study examines how reflections between the transducer and the skull as well as reflections within the skull will affect the phase by measuring the phase behavior along the propagation path of a single element.

2. Procedure

Experiments are conducted in an test tank filled with deionized water and padded with rubber to inhibit reflections from the tank walls. A 0.5 mm-diameter polyvinylidene difluoride (PVDF) hydrophone (Precision Acoustics, UK) is coupled with an ultrasonic PZT

* Corresponding author. Tel.: +1-617-278-0605; fax: +1-617-278-0610.

E-mail address: clement@bwh.harvard.edu (G.T. Clement).

0041-624X/01/$ - see front matter
PII: S0041-624X(00)00052-4

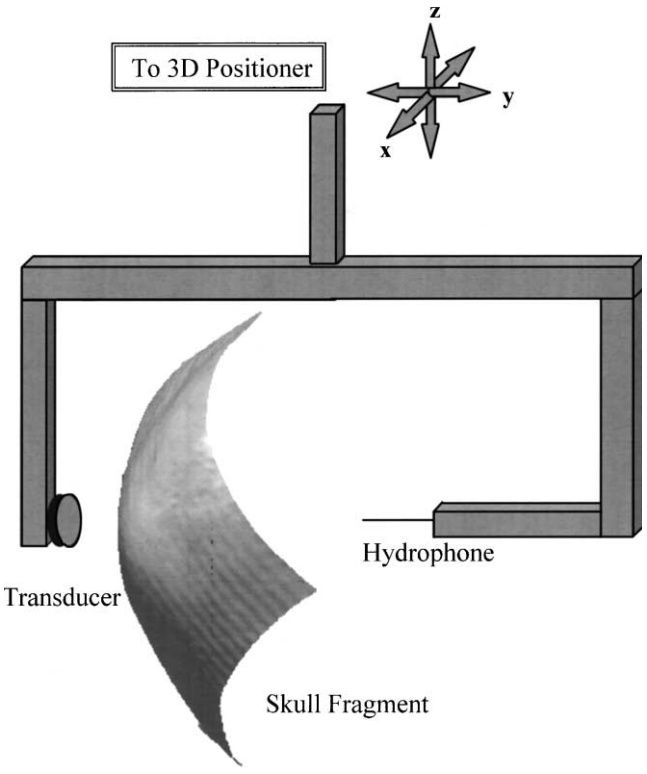

Fig. 1. Diagram of the coupled transducer/hydrophone system for measuring ultrasound propagated through the skull.

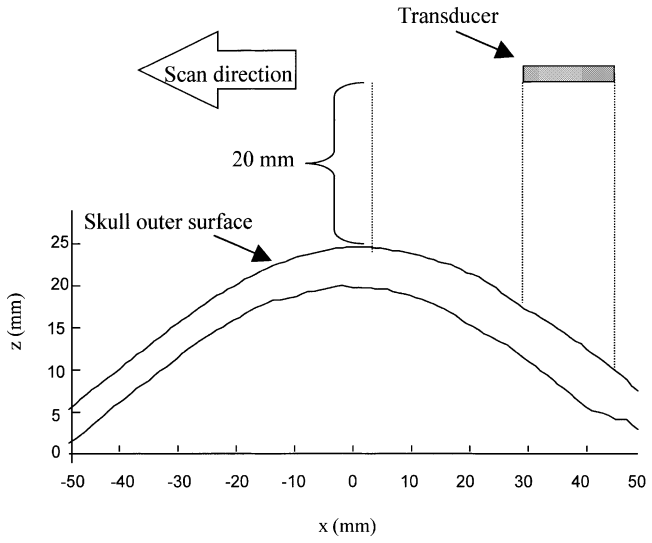

Fig. 2. Illustration of the transducer measurement directed along the skull surface.

planar transducer so that it maintains a constant distance from the transducer face along the undisturbed acoustic axis of propagation as depicted in Fig. 1. A circular 1.8 cm-diameter 0.5 MHz tungsten-backed transducer is used as the source. The transducer/hydrophone system is moved to arbitrary positions in the tank and rotated to arbitrary angles using a stepping-motor-controlled 3d positioning system (Parker, USA). The transducer signal is generated by an arbitrary waveform generator (Wavetek model 305) fed to a power amplifier (ENI). Hydrophone response is sent though a Precision Acoustics pre-amp into an amplifier (Preamble Instruments Model 1820) and recorded by a digital oscilloscope (Textronix model 680). Both the scan position and the data acquisition are computer controlled. Data from the scope is recorded at a specific time delay after the excitation of the transducer. Several cycles of the waveform beginning at the delay time are downloaded to a PC and Fourier transformed to obtain the phase of the resonant frequency.

Placing a skull fragment between the transducer and the hydrophone and scanning the coupled system along the axis perpendicular to the transducer face allows measurement of phase as a function of transducer distance from the skull. The skull is positioned so that the ultrasound angle of incidence is approximately normal upon the skull surface. Since the transducer and hydrophone are coupled as shown in Fig. 1, movement of the system along this axis should not disturb the directly propagated wave while causing changes in any reflected waves. Starting with the transducer in direct contact with the skull, the transducer is moved backward and the waveform recorded at 0.05 mm intervals. Driving signals of 10, 20 and 30 cycles and a continuous wave (CW) are input to the transducer. Use of the time-limited signals assists in determining the role of standing waves in the measured phase. The hydrophone is situated in the acoustic far field 11.4 mm from the transducer and the waveforms are recorded starting at 87.07 μs after the launch of the signal. In each experiment the scan process is repeated without the skull in place to measure the undisturbed phase and to assure the signal distortion is only due to propagation through the skull. A second set of measurements is performed by scanning along a line parallel to the transducer surface depicted as the x-axis in Fig. 2. A 100 mm length along the skull was sampled at 0.5 mm intervals, while the transducer is kept 2 cm from the distance of closest approach to the skull surface.

The hydrophone response is recorded as a function of the transducer distance from the skull surface allowing the acoustic phase of the driving frequency to be calculated. The fragment, which is fixed in formaldehyde is approximately 12 cm across and 18 cm from front to back. Based on a previous study [5] the acoustic properties of the skull were assumed to be similar to that of a fresh skull. In all calculations the speed of sound in the skull is taken to be $v = 2650$ m/s and the bone density is assumed to be homogeneous with a value of $\rho = 1796$ km/cm^3.

In order to compare the measurements to the theoretical model, it is necessary to obtain an accurate record

of the skull thickness and position. A map of the skull fragment is acquired using a laser-assisted mapping apparatus (manufactured in-house) depicted in Fig. 3. The device is mounted on the Parker positioning system and lowered along the z-axis until its probe comes in contact with the top surface of the skull. As shown in Fig. 3, contact causes the probe (C) to misalign an optical beam (M1), that is monitored with a photoresistor (P). The position along the z-axis may be recorded with a precision of about 50 μm. The process is repeated to form a surface map with a resolution of 1 pt/mm^2 in the $x-y$ plane. To obtain skull thickness a single side of the skull fragment is mapped with the device then the fragment is rotated 180° and the second surface mapped. Absolute distance between the inner and outer skull surfaces is determined using a caliper at four marked reference positions on the skull. To assure proper alignment, the fragment is mounted in a rigid holder. Through a series of 10 successive mappings, the mean standard deviation for all points was determined to be 0.38 mm. The incident angle between the transducer and the skull surface at each point is determined by first calculating the vector normal to the skull surface using two vectors on the surface, α_1 and α_2, taken using the third nearest neighboring points in the x- and y-directions. The scalar product between the resulting vector and the transducer surface vector β requires that the incident angle is

$$\gamma_i = \cos^{-1}\left[\frac{-(\alpha_1 \times \alpha_2)\cdot\beta}{|\alpha_1 \times \alpha||\beta|}\right]. \quad (1)$$

Simulated data is calculated assuming multiple reflections between the skull and the transducer as well as internally within the skull. The field at a specific point is then determined from the argument of the integral of the pressure over the interior wall of the skull. Detailed description of the theory is provided in an ensuing appendix section.

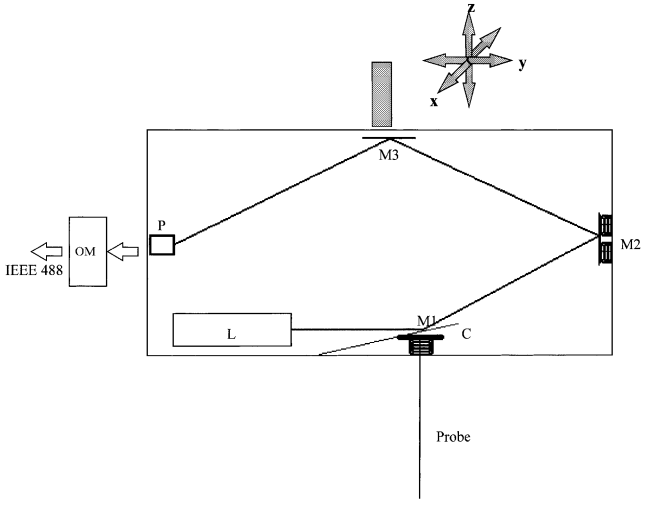

Fig. 3. Diagram of the surface-mapping probe. The probe is mounted on a stepping motor controlled positioning system and records displacement of the probe end with a precision of approximately 50 μm.

3. Results

The phase measured across a 20 cm line along an initial scan direction parallel to the transducer face (Fig. 2) is presented in Fig. 4a along with its corresponding simulation. The mean difference between the measured and simulated points is 1° and the standard deviation across all points is determined to be 11.6°. The discrepancy between the simulated and measured phase is largest at the edge of the scan where the incident angle of the ultrasound upon the skull surface becomes larger. The discrepancy becomes more pronounced as the scan continues outward toward the edge of the skull sample. The phase measured over a longer, 100 mm scan is presented in Fig. 4b where model used in this paper fails due to the increasing importance of mode coupling not considered in the model. Across the 100 mm scan the mean difference between the experiment and the simulated phase data is 7° with a standard deviation of 52°.

An important result of the simulation is illustrated by considering reflections within the skull. The phase of the propagated signal, regardless of the angle of incidence, deviates only slightly from the limiting case consisting of no reflection. The simulated phase as a function of incident angle in presented for a 0.5 MHz wave across a

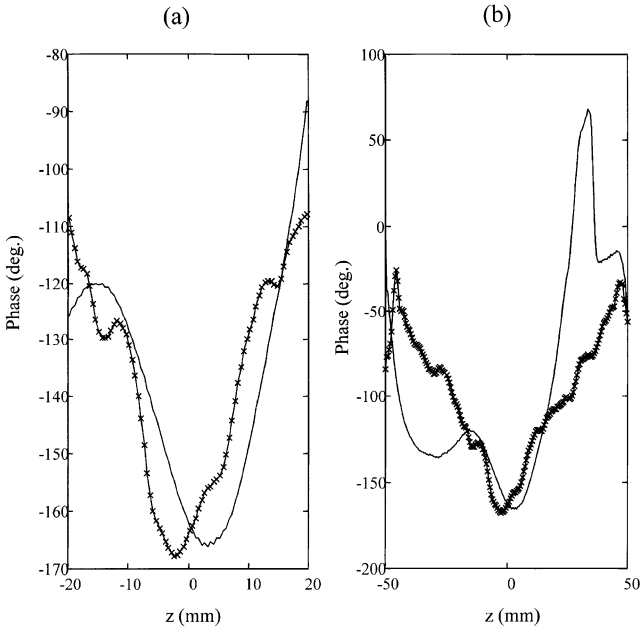

Fig. 4. Transskull ultrasound phase along line × parallel to the transducer face over (a) a 20 cm length and (b) a 50 cm length using a 0.5 MHz transducer. The crossed line represents an experimental measurement and the solid line is numeric.

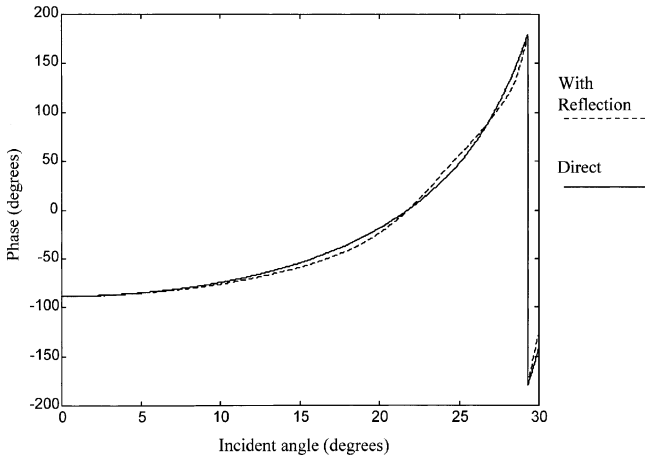

Fig. 5. Simulation of the expected phase contribution due to reflections inside the skull (- - - - -) compared to the result neglecting internal reflection.

homogeneous 3 mm-thick skull bone in Fig. 5. Comparable results were obtained simulating bone thickness from 0 to 6 mm over the frequency range of 0.5–2 MHz.

The next measurement direction was directed along the z-axis, normal to the transducer face. The phase of the pressure field at the hydrophone as a function of transducer distance from the skull is presented in Fig. 6a with the transducer driven in continuous mode. Periodic variation in the phase with a peak differential of 25° is found over the measured distance. The simulated phase at the hydrophone is found to be equal to $-132°$ while the experimental phase at this distance is found to be $-146°$ for both the 30-cycle and the 20-cycle data, $-135°$ for 10 cycles, and $-131°$ for CW. Time-limited signals are presented in Fig. 6b–d showing that this variation can be eliminated by using short bursts and longer distances from the skull.

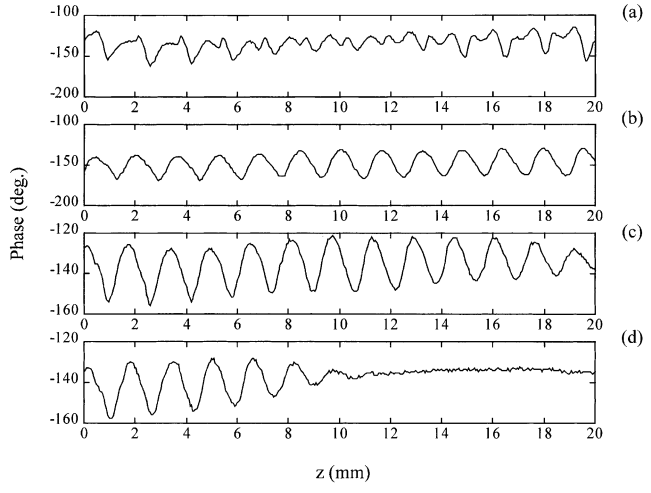

Fig. 6. Phase variation as a function of distance from the skull surface at (a) CW, (b) 30-cycles, (c) 20-cycles, (d) 10-cycles.

4. Discussion

While the measured and simulated plots in Fig. 4a appear somewhat offset along the position axis, their values do not deviate from each other beyond a maximum of 20° in phase. It is evident from Fig. 4b that the experimental measurements of transcranial ultrasound phase as a function of incident angle and deviates from the expected results at high incidence. This discrepancy is not believed to result from reflections within the skull bone but rather from the breakdown of two assumptions of the simulation model: (i) At higher angles the inner and outer skull surfaces can no longer be considered parallel and (ii) mode coupling is no longer negligible. Due to the discrepancy, the current study refers only to the case of small ($<10°$) incident angles.

The standing waves between the skull and the transducer had an effect on the phase, causing the phase of transskull propagated pressure to shift by as much as 25°, depending on the distance between the skull and the transducer. Since the field from a transducer array is the superposition of the complex pressure field of individual sources, knowledge of the behavior of a single transducer, such as the phase measurements obtained in this study, generalize the multi-element case. In the case of multi-element therapeutic array, standing waves could shift each element by up to 25° depending on its distance for the transducer. A previous study suggests that phase shifts of this magnitude will not have a significant effect on the formation of a single focus through the skull [6]. However the data indicates that if required, the reflection-induced phase distortions may be eliminated by reducing the number of cycles in the signal and increasing the transducer distance from the skull. For example, the phase at the hydrophone resulting from 10-cycle burst (Fig. 6d) is independent of the distance from the skull for distances greater than 10 mm. Beyond this distance the time of flight of the directly propagated and reflected waves is large enough to prevent the waves from interfering. Thus, positioning all elements of a transducer array at a distance greater than the signal's burst length from the skull may simplify phase prediction for therapeutic applications.

5. Conclusion

Accurate focusing of ultrasound after transcranial propagation requires knowledge of the phase throughout the desired focal region. It is therefore important that the role of reflections in the distortion of the phase be understood. For the case of a 0.9 cm-radius transducer at 0.5 MHz, we have found that reflections can cause appreciable change to signals when the transducer is placed very close to the skull. However, moving the transducer away from the skull and limiting the ultra-

sound pulse duration results in a signal independent of skull position. The simple model of reflections at interfaces was able to predict phase after ultrasound propagation through the skull for small incident angles. Reflections within the skull bone are not expected produce appreciable effects on the propagated phase regardless of the entrance angle of the ultrasound. Results indicate that standing waves caused by reflections between the transducer and can have a measurable contribution on the phase of the wave propagating through the skull. However this contribution is less than 25° for the 0.5 MHz signal considered. Additionally it is demonstrated that this contribution can be eliminated using a multi-cycle pulse away from the skull surface as an alternative to a CW signal.

Acknowledgements

Support for this study was provided by grant no. 1R01CA7650-01 from the National Institutes of Health.

Appendix A. Reflection model

The model considers skull propagation as two separate transmission problems. The first considers reflections between the transducer and the skull surface and the second considers reflections within the skull bone situated between two water layers. The skull is treated as a homogeneous material and mode coupling is neglected. Further, the skull bone thickness is assumed to vary slowly over an ultrasound wavelength, and the tangents to the inner and outer surfaces of the skull are assumed parallel. Justification of these assumptions and the limitations of this model are discussed in Section 4. Under these limiting conditions the skull is modeled as having a constant thickness over the beamwidth and the transmitted power at each interface is expressed as,

$$T = \frac{4\left(\frac{\rho_1 c_1}{\rho_2 c_2}\right)\left(\frac{\cos\theta_t}{\cos\theta_i}\right)}{\left[\left(\frac{\rho_1 c_1}{\rho_2 c_2}\right) + \left(\frac{\cos\theta_t}{\cos\theta_i}\right)\right]^2}, \tag{A.1}$$

where ρ_1 is the density of the incident medium ρ_2 is the density of the transmission medium. The speed of sound in the incident and transmission medium are c_1 and c_2, respectively. The incident angle of the ultrasound beam upon an interface is given by θ_i and θ_τ is the refracted angle which may be eliminated from Eq. (A.1) using Snell's law.

Reflections in the water bath between the transducer and the skull surface are determined by successive application of Eq. (A.1) for each reflection. Eq. (A.1) is applied to both the PZT–water interface T_1 and the water–skull interface T_2:

$$\Delta\phi_w = \arg\left(T_1 T_2 \sum_{n=0}^{\infty} (1-T_1)^n (1-T_2)^n \times \exp\left[\mathrm{i}2(2n+1)kL/\cos\theta_t\right]\right), \tag{A.2}$$

where k is the wavenumber in water, L is the distance from the transducer to the skull surface and n is the reflection number, $n = 0$ representing the directly propagated wave.

The assumption that the skull bone is constant across the incident ultrasound beam limits the validity of Eqs. (A.1) and (A.2) to cases of a narrow planar beam. However, the equations serve as an adequate comparison of the experimental data in this paper which is limited to studies involving planar sources less than 2 cm in diameter having wavelength of 3 mm in water.

Upon passing through a skull area of thickness L the wave will experience an additional phase shift determined from the argument of the series,

$$\Delta\phi_s = \arg\left(T^2 \sum_{n=0}^{\infty} (1-T)^{2n} \times \exp\left[\mathrm{i}2(2n+1)k_s L_s/\cos\theta_t\right]\right), \tag{A.3}$$

a simplification of Eq. (A.2) since the transmission coefficient T is the same at both interfaces.

Ultrasound phase at the hydrophone may be determined from the argument of the integral of the pressure over the inner wall of the skull,

$$\Delta\Phi(r) = \arg\left(\frac{1}{S'}\int_S P(r')\exp\left[\mathrm{i}\Delta\phi(r')\right] \times \exp\left(\mathrm{i}k|r-r'|\right)\mathrm{d}S'\right), \tag{A.4}$$

where r is the distance from the transducer to the hydrophone and r' is the distance from the hydrophone to the surface element $\mathrm{d}S'$ and $S' = r\lambda$.

References

[1] K. Hynynen, F.A. Jolesz, Demonstration of potential noninvasive ultrasound brain therapy through an intact skull, Ultrasound Med. Biol. 24 (1998) 275–283.
[2] J.-L. Thomas, M.A. Fink, UItrasonic beam focusing through tissue inhomogeneities with a time reversal mirror: application to transskull therapy, IEEE Trans. Ultrason. Ferroelectr. Freq. Contr. 43 (1996) 1122–1129.
[3] M. O'Donnell, S.W. Flax, Phase aberration measurements in medical ultrasound: human studies, Ultrason. Imaging 10 (1988) 1–11.
[4] J. Sun, K. Hynynen, Focusing of therapeutic ultrasound through a human skull: a numerical study, J. Acoust. Soc. Am. 104 (1998) 1705–1715.
[5] F.J. Fry, J.E. Barger, Acoustical properties of the human skull, J. Acoust. Soc. Am. 63 (1978) 1576–1590.
[6] H. Wang, E. Ebbini, C.A. Cain, Effect of phase errors on field patterns generated by an ultrasound phased-array hyperthermia applicator, IEEE Trans. Ultrason. Ferroelectr. Freq. Contr. 38 (1991) 521–531.